Towards renewable public transport: mining the performance of electric buses using solar-radiation as an auxiliary power source

Haoqian Chen[a], Yi Sui[a,b,*], Wen-long Shang[c,d], Rencheng Sun[a], Zhiheng Chen[b], Changying Wang[a], Chunjia Han[e], Yuqian Zhang[f], Haoran Zhang[g,b]

[a] College of Computer Science and Technology, Qingdao University, Ningxia Road No.308, Qingdao 266071, China

[b] Center of Spatial Information Science, The University of Tokyo, 5-1-5 Kashiwanoha, Kashiwa-shi, Chiba 277-8568, Japan

[c] Beijing Key Laboratory of Traffic Engineering, College of Metropolitan Transportation, Beijing University of Technology, Beijing 100124, China

[d] School of Traffic and Transportation, Beijing Jiao tong University, Beijing100044, China

[e] Department of Management, Birkbeck, University of London, London WC1E 7HX, United Kingdom

[f] China Institute of Marine Human Factors Engineering, Yingshanhong Road No.117, Qingdao 266400, China

[g] School of Business, Society and Engineering, Mälardalen University, Västerås 721 23, Sweden

*Corresponding author: Yi Sui: suiyi@qdu.edu.cn

Abstracts:

Transforming the road public transport to run on renewable energy is vital solution to achieve carbon neutral and net zero goals. This paper evaluates the potential of using solar radiation-generated electricity as an auxiliary power supplementary for the battery of electric buses, based on a developed framework that using publicly street-view panoramas, GPS trajectory data and DEM data as input parameters of solar radiation model. A case study of Qingdao, China with 547 bus routes, 28661 street-view panoramas shows that the solar-radiation electricity generated at noon during the operation accounts for about one-fourth, one-sixth of the total electricity consumption of a bus traveling one kilometer in a sunny day and a cloudy day, respectively. Spatial variability shows significant solar-radiation power generation advantages in newly-launched areas and expressway. The solar power generated in a sunny day can make a bus full of passengers and with air conditioner on at least one extra trip in 2:1 replacement schedule and 4:3 replacement schedule. A correlated relation between the solar-radiation power generation benefit and the operation schedule of electric buses is observed, implying that the high cost of 2:1 replacement schedule for long-distance routes during summer or winter can be reduced. The proposed framework can help us evaluate and understand the feasibility of solar radiation-generated electricity energy of electric bus fleets covering the large-scale urban areas at different times, locations, and weather conditions, so as to support effective decisions at better planning of PV-integrated electric buses.

Keywords: Electric buses, Solar radiation-generated electricity, Spatio-temporal distribution, Operation schedule

Highlights:

- Developing a framework to estimate solar PV potential of urban fleet-wide electric buses.
- Publicly street-view panoramas, GPS trajectory data and DEM data are used as input.
- A case study of Qingdao, China with 547 bus routes, 28661 street-view panoramas is studied.
- Benefits under different driving conditions and operation schedules are evaluated.

1. Introduction

1.1 Background

Reaching well-below 1.5°C and 2°C goal of the Paris Agreement require global CO_2 emissions to drop to net zero around mid-century[1]. As the road transport sector contributes significantly to global carbon emissions[2], which have been rated by many countries as the fastest-growing emitter [3], the electrification of vehicles and the shift to public transport are widely regarded as viable strategies to meet the goals of Paris Agreement[4]. With rapid advances in technology and policy incentives, global electric vehicle fleet exceeded 5.1 million in 2018, up by 2 million since 2017[5]. Electric buses constitute the fastest-growing part of the electric vehicles market[6]. As of the end of 2017, around 380,000 electric buses were plying the streets of cities in China, most of which were pure battery electric buses[7]. Beyond China, in Europe 50 cities and regions have signed "European Clean Bus deployment Initiative" and make combined efforts to increase the share of fossil fuel-free buses to 30% in 2025[8]. In United States, new buses purchased in California must be "zero-emission" by 2029 and all buses will be fully electrified by 2040[9].

Large-scale deployment of electric buses come with enormous demand for electricity, which poses a significant challenge to the grid[10]. The power consumption per kilometer operation of an electric bus was mostly influenced by the ambient temperature (summer or winter, etc.), driving behavior (frequent stop-and-go operation), and route characteristics (steep gradients)[11]. With the passengers' expectations related to standards of travel comfort rise, the non-traction needs of electric buses, such as heating and air condition, significantly contributes to the increase of consumption of electric energy[12]. A case study in Singapore showed that a fully electric bus fleet covering 350 bus routes with more than 5000 buses required about 1.4GWh per day for revenue service[13]. As a result, on one hand, charging needs of electric buses poses extra burden to the electrical supply, particularly during peak electricity consumption periods; on the other hand, high power demand from non-traction systems not only greatly reduces the daily mileage of buses, but also increases the risk of deep discharge of the battery in rush hours[14].

In many cities, a mixture of slow charging at night with one or various fast charges (including opportunity charges and ultrafast charges) during a day is widely employed. When opportunity charging end-of-route is employed, additional buses are dispatched to maintain the service during this period. With high rate of power (up to 600kW) provided by ultrafast chargers, the charging time can be reduced to 10-40 seconds, so that high-power chargers can be installed at various bus stops to charge when passengers get on and off, which is called opportunity charge en route. Ultrafast charging was considered as a useful approach of battery supplement and maintain the service level without causing schedule delays[15]. In addition, the wirelessly charged battery can be downsized and thus induced a reduction of battery-to-wheel energy consumption[16, 17]. However, it is not feasible to widely deploy in urban area due to high infrastructure cost and limited route flexibility. Thus, there is an urgent need to equip external power supply system to charge.

As renewable and sustainable energy, solar photovoltaic (PV) has long been thought as a competitive power source[18]. The corporation of PV systems and electric buses seems more attractive. Bus usually has large body area, such as a flat roof with a length of 10-12m and width of 2-3m, which provides ideal surface for installing PV modules. Lightweight thin-film solar cells can be installed on the flat rooftops, which have little effect on the overall weight of the bus and then will not have a negative impact on efficiency of electric usage[19]. Planning to introduce of PV-integrated buses into the existing public transport networks requires careful consideration. Recently, research efforts conducted on lab scale[20, 21] and several standard routes in urban area [14, 22, 23] have proved that the integration of PV modules on electric buses was a viable approach to extend daily mileage or battery cycle life. Although PV-integrated electric bus sounds feasible, the actual performance of PV-integrated buses largely relates to the capacity of solar radiation generation, which heavily depends on the surrounding environment in which bus travels around. Solar irradiation may change significantly within short distances due to varying elevation, surface orientation and shadows. As shown in Fig.1, the potential solar PV of electric buses depends on sun position, surface characteristics (latitude, elevation and orientation), and shadows cast (caused by buildings and trees). Accurately evaluating solar radiation-generated electricity energy of electric bus fleets covering large-scale urban area at different times, locations and weather condition is not an easy task. Therefore, it is of interest to evaluate the potential of using solar radiation-generated electricity energy as auxiliary power supplementary for batteries.

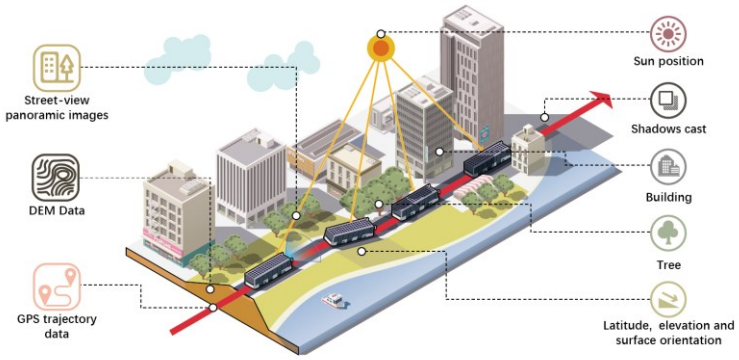

Fig.1 The environmental influence on the potential solar PV of electric buses

Earlier works usually installed insolation sensor on test buses to measure solar irradiation. Although solar radiation measured through insolation sensor is accurate, fiscal resources required in the data collection limit its application in fewer buses, which cannot provide sufficient decision support for planning and deployment of large PV-integrated electric bus fleets at a metropolitan-wide scale. Another approach is to adopt available solar resource maps which is estimated by extrapolation of point-specific measurements to obtain solar irradiation. Using average solar irradiation value is simple, however, it yields a rough estimation and ignores the heterogeneous surrounding environment characteristics on a local scale, which is difficult to provide an accurate estimation of solar irradiation.

In this study, we develop a method framework by employing street-view panoramic images, GPS trajectory data of routes, and DEM (Digital Elevation Model) data as input to solve the above problem. As shown in Fig.2, based on the proposed framework, we dedicate to answer the following

research questions: (1) what are the spatio-temporal characteristics of solar power generated by PV-integrated buses at a metropolitan-wide scale? For example, rush hours v.s. non-rush hours, downtown v.s. newly built areas. (2) as a supplementary power source, how much mileage can be extended by the solar radiation-generated electricity energy, taking into account the various driving situations of passenger load and air conditioning usage? (3) what supplementary benefits do PV-integrated buses have under different operation schedules? For example, on-duty along routes and off-duty in parking lots. A case study in Qingdao, China is studied to answer these questions, which can help us understand the feasibility of fleet-wide planning of PV-integrated buses, so as to support effective decisions at the deployment of PV-integrated electric buses at city-wide scale.

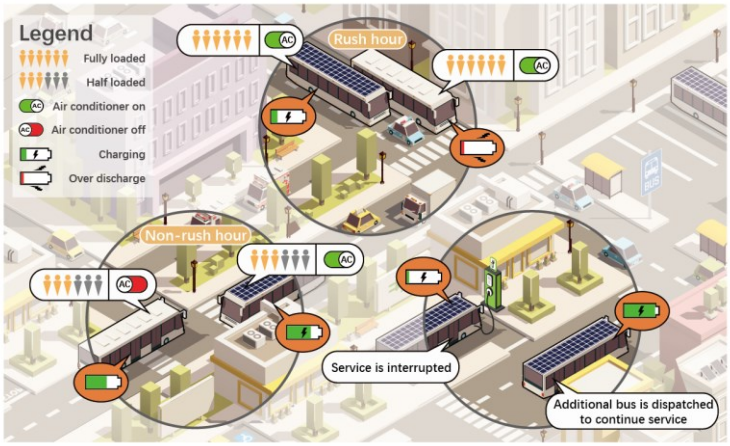

Fig.2 The research questions in this study

1.2 Literature review

Many research efforts have been put into the use of PV panels as an energy source for passenger cars and buses. Estimation of solar power generated by the PV panels is key aspect. Solar radiation is time, location, elevation, surface orientation and shadows dependent, which is determined by local environment. The most effective approach of acquiring the solar radiation value is to measure by on-board equipment. Insolation sensor can be equipped on the vehicle body to record the solar irradiation accurately. For example, a plug-in hybrid car was equipped a pyranometer to measure the electric power that can be generated by 6.8m^2 PV modules on rooftop and side doors[24]. The recorded data collected under in real-world driving condition in100 days showed that PV modules can generated average 2.1 kWh electricity per day. In [20], semi-flexible polycrystalline modules consisted of 464 cells of rated power of 4.06W were installed on the rooftop of a moving bus. A two-month standard drive cycle operation showed that the PV system can generate 418kWh electric energy during this period, which was close to 18% of the bus demand for electricity. Insolation sensor presents accurate measurements, however, it is not feasible for a large number of buses in city due to high cost.

A few works adopted readily available solar resource maps saved in database to acquire the solar irradiation. The widely used databases include SOLARGIS[25], time and day database[26], Typical Meteorological Year[27], *etc*.. These databases provide macroscopic estimates of solar radiation by city or region. For example, a case study in Invercargill, New Zealand used the hourly beam and diffuse irradiation data, the position of the sun from time and day database and TMY files to estimate the solar irradiation generated by installing solar panels on the rooftop of electric bus[23].

The weighted average yearly solar irradiation can reach 8.5% of the total annual energy demand of the electric bus. In [21], hourly solar irradiance values for Delhi region were used for estimating power produced by solar panels installed on a light-weight bus body. Solar technology with lightweight design bus can save 31% of the energy consumption compared to conventional electric bus. The readily solar irradiation data is easy to use, however, the estimation accuracy is limited. Because these data represent roughly estimation of a city or area through interpolating or extrapolating from point-specific measurements, which cannot provide reliable estimation in the complex streetscape with various surface features.

Solar models provide a cost-efficient means for estimating the spatial and temporal variation of solar insolation over given location or area. Solar models usually use features of the PV installation surface as input, i.e. site latitude and elevation, surface orientation, shadows cast by surrounding topography, daily and seasonal shifts in solar angle, and atmospheric attenuation[28]. The parameter of the area exposed to the sun in model is extremely important in estimating solar radiation, which is usually represented by sky view factor (SVF). SVF was originally defined as the ratio of radiation received from sky to that received from the entire hemisphere radiation environment[29], and can be simplified as a value between 0 to 1, representing the ratio of the unobscured area of the upward-looking hemispherical (fisheye) photograph from a given surface point[30]. In [14], a static SVF value was used to estimate the solar energy generated from roof-mounted and full body-mounted electric buses. However, this simple assumption cannot reflect real SVF of a running bus in streetscape. In order to obtain the accurate value, Digit Surface Model (DSM) that includes detailed footprint and height information of buildings and trees along the street is widely used. The generation of DSM depends on high-precision 3D building and topography databases. For example, a high-resolution aerial image (0.25m) was adopted to segment trees and then trees information were combined with building footprint and height to generate DSM for calculating sky coverage map [22]. By considering the real-world surface features, DSM-based method can obtain more accurate estimation. However, this method requiring high-resolution aerial image is inherently limited with respect to feasibility. Another way to calculate accurate SVF is to use ultra-wide angle camera installed on the top of the vehicle to capture street-view panorama images. A field test studied the solar potential of PV-integrated bus in New Zealand through installing a high-definition 360 camera on rooftop of a vehicle driving on a bus route[23]. 22 fisheye images with 256×256 pixel size were obtained at fixed sample points. Considering the time and effort cost, taking panorama images by onsite camera is suitable only for small-scale study.

With the advantage of densely coverage in nearly every urban street, the freely accessible street-view panorama images provided by web companies, such as Google and Baidu, become a low-cost and effective alternative to the onsite camera approach. SVF estimates from street view panorama images has proved to be very consistent with the estimation from LiDAR-based DSM and oblique airborne photogrammetry-based 3D city model[31], and the marching degree is quite satisfactory even in a high-density urban environment[32]. Based on street-view panorama images, the potential solar irradiance of street canyons in different cities were studied, such as Hong Kong[33], Boston[34] and Xi'an[35], which strengthens our understanding of the viable of use of solar energy to promote sustainable cities. However, the above literature does not relate with the potential of solar power generation by PV-integrating buses traveling around city-wide area. A similar study, where predicting and calculating the solar radiation and electric energy that can be collected from roads, is presented in [36]. While the authors used street-view panorama images to

estimate solar power of roads, which inspired our research, their study goals were quite different from ours. In addition, the calculation of incidence angle in solar model was simplified, resulting in inaccurate results.

1.3 Contribution of this work

In summary, the main contributions of this study are three folds:

(1) This paper proposes a method framework for estimating solar radiation-generated electricity energy of fleet-wide PV-integrated electric buses traveling around city-wide area during different times and weather conditions. Detailed procedure for obtaining spatio-temporal characteristics of solar radiation generation of PV-integrated electric buses is given. The methodology presented in this study can be used in different cities or areas to support deployment decision of PV-integrated electric buses.

(2) The potential analysis of generating solar power that can be used for operation through alternatively service (on-duty on road and off-duty at parking lot) is discussed, in which real driving conditions (passenger load and air conditioner usage) are taking into account to evaluate the power saving benefits of PV-integrated electric buses.

(3) Scenario analysis and a general discussion of the impact of operation schedule on the solar power generation of PV-integrated electric buses are given, which can help understand the supplementary benefits of PV-integrated electric buses under different operation schedules.

The remainder of the paper is organized as follows: Section 2 provides our methodology. Study area and data preprocessing are given in Section 3. In Section 4, empirical analysis and scenario analysis are provided. We discuss our findings and implications in Section 5. Finally, we conclude our study and discuss future research in Section 6.

2. Methodology

2.1 Overall research framework

This study aims at conducting a generalized process to calculate the solar radiation-generated electricity energy of a PV-integrated electric bus when running on the road and parking at lot. First, geographical information of routes including stops and trajectories along roads are used as input to obtain street-view panoramic image through acquisition engines (Baidu API or Google API). Secondly, the street panoramas are transformed into fisheye images by hemispherical projection, and the transformation results are segmented to obtain foreground area (visible sky pixels) and background area (non-sky pixels). Third, based on the binary classification results, gap fraction (proportion of sky areas) is calculated as an input parameter for solar model. In addition, DEM data (elevation) are used to estimate the slope and aspect of surfaces, which are fed into solar model to calculate incidence angle of sunlight reaching the surface. According to the Sunmap & Skymap provided by the solar model, direct solar radiation and diffuse solar radiation can be estimated. After the above process, spatio-temporal analysis of solar irradiation can be conducted, and then the potential solar power generation of buses during operation and parking at lot can be analyzed. Finally, scenario analysis of different replacement modes of electric buses and conventional buses are studied in order to understand the supplementary benefit of PV-integrated electric buses under different operation schedules. Passenger load and air conditioner usage are considered in the above analysis in order to reflect real operation situations. The overall research flow is shown in Fig.3.

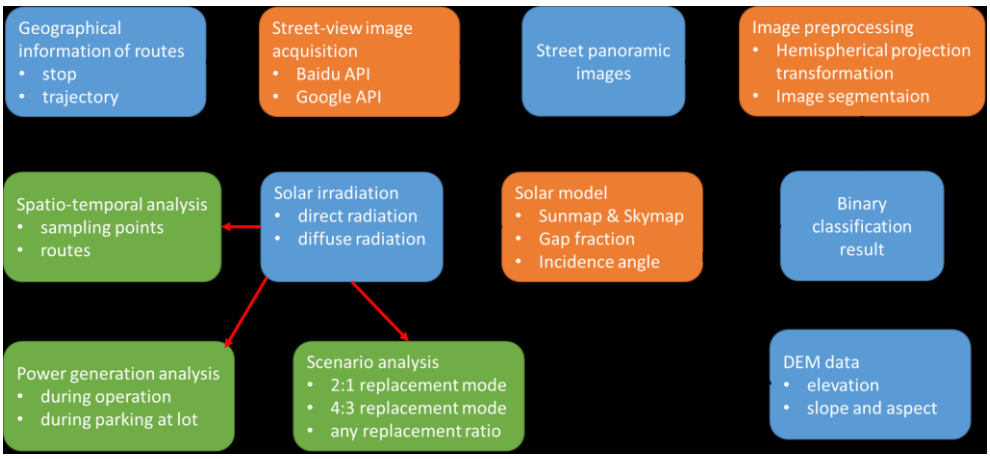

Fig.3. Research flow chart

2.2 Street panoramas acquisition and process

Street-view panoramic images record a complete real viewing of the world for a ground location, which are often captured by omnidirectional cameras, providing an entire viewing sphere surrounding its optical center. Through Google Street View (GSV) API or Baidu Street View (BSV) API, street-view panoramas of most cities around the world can be retrieved. For example, given the latitude-longitude coordinate and other parameters, such as horizontal field of view, compass heading, and up or down angle, the GSV API can return the closest available panorama image of the ground location.

For estimating solar radiation at a ground location, using the method in [34], panoramic images are first converted to hemispherical field of view to acquire an upward-looking view of the sky. Each position of the hemispherical projection corresponds to a sky direction, with the zenith in the center and the horizons at the edges. We use equiangular projection for a full 180-degree field of view, that is, the zenith angle is proportional to the distance along a radial axis [37]. Note that east and west are reversed due to the upward projection. Fig.4 illustrates the hemispherical projection of panoramic image, the result of which is often referred to as a fisheye image.

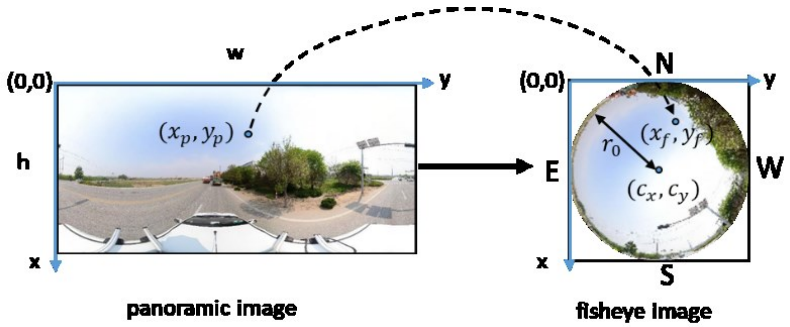

Fig. 4. Hemispherical projection from panoramic image to fisheye image

More formally, let w and h be the width and height of panoramic image I_p, respectively. The radius of the converted fisheye image I_f is $r_0 = w/2\pi$, and the center coordinates of I_f is (c_x, c_y), where $c_x = c_y = r_0$. Every pixel at (x_p, y_p) in I_p can be converted to corresponding coordinated point (x_f, y_f) in I_f by $x_p = w\theta/2\pi$, and $y_p = hr/r_0$, where (r,θ) is polar coordinate of point (x_f, y_f).

$$r = \sqrt{\left(x_f - c_x\right)^2 + \left(y_f - c_y\right)^2} \tag{1}$$

$$\theta = \begin{cases} \frac{\pi}{2} + tan^{-1}\left(\frac{y_f - c_y}{x_f - c_x}\right), & x_f \le c_x \\ \frac{3\pi}{2} + tan^{-1}\left(\frac{y_f - c_y}{x_f - c_x}\right), & x_f > c_x \end{cases} \tag{2}$$

The solar radiation for a ground location is the sum of irradiation values from all sky directions that are not obscured. Next, fisheye images are segmented to extract visible sky regions. U-Net [38] is an encoder-decoder convolutional neural networks (CNNs) architecture for fast and precise segmentation of images, which has been proved as a state-of-the-art solution to many computer vision tasks, such as PV panel semantic segmentation[39, 40]. Ideally, segmentation task on fisheye images can inherit pre-trained U-Net on tremendous data and annotation directly, however, heavy distortions in the polar regions of fisheye image hinder vanilla encoder-decoder CNNs to compute feature patterns well with fixed kernel over the entire image [41]. To overcome this challenges, existing literatures either 1) simulate the fisheye effect by applying a distortion on perspective image datasets, such as Cityscapes or SYNTHIA in order to gather numerous training data with ground truth [42] or 2) collect numerous real fisheye images and annotate them manually which is time-consuming and undesirable. In this study, we focus on visible sky regions and then the segmentation task can be simplified into binary classification task: foreground (visible sky pixels) and background (non-sky pixels). As the feature patterns of the foreground are significantly different from the background, segmentation performance can reach good level with a few training datasets and annotations. We annotate 50~ fisheye images from nearly 30,000 fisheye images dataset to train the U-Net model, and the segmentation performance is good.

2.3 Solar radiation model

Solar radiation is emitted by the sun through the atmosphere, and can be mainly divided into two types: direct radiation that passes unimpeded through the atmosphere from the sun, and diffuse radiation that is scattered by the atmosphere. According to solar radiation model proposed by Rich [37, 43], both two types of solar radiation for a ground location depend upon the relative position of the sun, gap fraction, incidence angle, and atmospheric conditions.

(1) The relative position of the sun

Direct sunlight moves regularly from winter solstice to summer solstice (December 22 to June 22) and from summer solstice to winter solstice (June 22 to December 22) every year. The position of the direct sunlight varies with time, which can be specified by Sunmap. As shown in Fig.5(a), the Sunmap consists of discrete sky sectors, and the interval between left and right adjacent sectors is half hour, and the interval between upper and lower adjacent sectors is one month. For example, the moving path of the sun on the day of equinox at 36° N latitude consists of 24 sectors, with sunrise starting around 6 am and sunset around 18 pm. The direct sun radiation over any time interval interest can be calculated based on Sunmap.

Unlike direct solar radiation, which only originates from directions along the sun track, diffuse radiation can originate from any sky direction due to the scattering of gases, dust, aerosols and other substances in the atmosphere. In order to estimate diffuse sun radiation, all visible sky directions

should be taken into account. For simplification, the Skymap divides the whole sky into a series of sky sectors, as shown in Fig.5 (b). The diffuse sun radiation is the sum of diffuse radiation value from all visible sky sectors. Obviously, the Skymap specifies the variations of solar radiation in space.

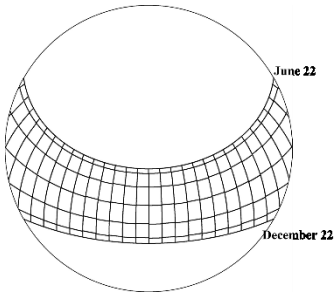

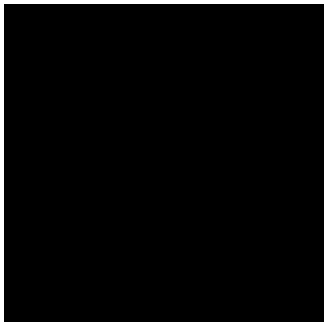

(a) (b)

Fig.5 (a) Sunmap at 36° N latitude with sun track from winter solstice to summer solstice and (b) Skymap defined by 4 zenith divisions and 8 azimuth divisions

The relative position of the sun for each sky sector in Sunmap and Skymap is defined by zenith angle (z) and azimuth angle (α) at the sector center. The zenith angle (z) and azimuth angle (ω) of the centroid (x,y) of each sky sector are calculated as follows:

$$z = arcsin\sqrt{\frac{x^2+y^2}{r_0}} \tag{3}$$

$$\omega = \begin{cases} arcsin\dfrac{x}{\sqrt{x^2+y^2}} & x>0, y>0 \\ 90° + arccos\dfrac{x}{\sqrt{x^2+y^2}} & x>0, y<0 \\ 180° + arcsin\dfrac{-x}{\sqrt{x^2+y^2}} & x<0, y<0 \\ 270° + arccos\dfrac{-x}{\sqrt{x^2+y^2}} & x<0, y>0 \end{cases} \tag{4}$$

where (x,y) is the coordinate of the fisheye image with center (0,0) at the zenith.

(2) Gap fraction

Gap fraction is the proportion of visible sky within a given sky sector. A gap fraction of 0 means the sky sector is completely blocked, and 1 means it is completely visible. The solar radiation of a sky sector is proportional to unobstructed visible sky area of that sector. Combined with segmented fisheye images, gap fraction for a sky sector can be calculated. Fig.6(a) is the overlap of fisheye image and the Sunmap on the equinox day at 36° N latitude. From 17:00 to 18:00 p.m, the right sectors that the sun track located are blocked, and the completely blocked sectors (shown in black color) do not receive any direct solar radiation. Similar, the overlap of fisheye image with the Skymap is shown in Fig.6(b), the diffuse solar radiation of a sky sector depends upon the proportion

of the visible sky area of that sector.

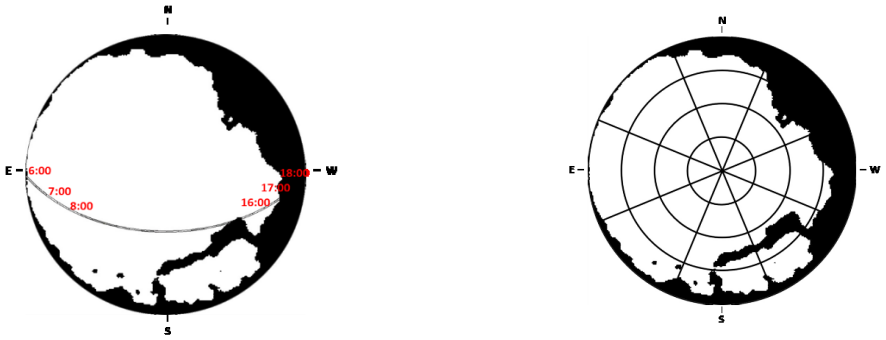

(a) (b)

Fig.6 (a) Sunmap at 36° N latitude overlapped with segmented fisheye image and (b) Skymap overlapped with segmented fisheye image

(3) Incidence angle

As shown in Fig.7, given a sky sector center at O with zenith angle z and azimuth angle ω, incidence angle θ is the angle between a surface and incoming sunlight reaching the surface. Line Og is a plumb line representing zenith. The amount of solar radiation reaching the surface is proportional to the cosine of the incidence angle θ. When the incidence angle θ is close to zero, the surface receives the full amount of solar radiation; whereas the angle is close to 90 degree, the surface receives no solar radiation. The value of $cos\,\theta$ for a ground surface depends upon the zenith angle z, the azimuth angle ω, and the slope representing the rate of change in elevation for that surface. In the Fig.7, slope is denoted by angle α.

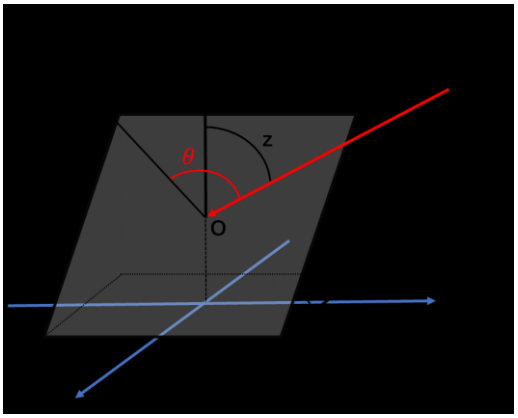

Fig.7 Relationship between incidence angle, zenith angle, azimuth angle and slope of a surface. Line Of is surface normal and Og is a plumb line representing zenith.

In order to calculate $cos\,\theta$, the incident direction of sunlight is divided into four ranges, starting from due north and clockwise from 0°~90°, 90°~180°, 180°~270° and 270°~0°, as shown in Fig.8. For each range, $cos\,\theta$ can be calculated as

$$cos\,\theta = \cos\alpha\cos z - \sin z\sin\alpha\cos\omega \tag{5}$$

Some reference lines and planes are marked in Fig.8 for understanding the Eq.(5). Let plane H

be parallel to the horizontal ground. The red line cO represents the sunlight reaching the surface. Make a vertical line from point f that is perpendicular to H and the intersection is represented by point e. The aspect of the surface is directed by line Oe (due south). From point c make a line parallel to fe and intersecting point b at H. Starting at point c, make another line cd parallel with line Of. The lines oe, ob, od and bd are on plane H. Note that the aspect of a surface points to due south.

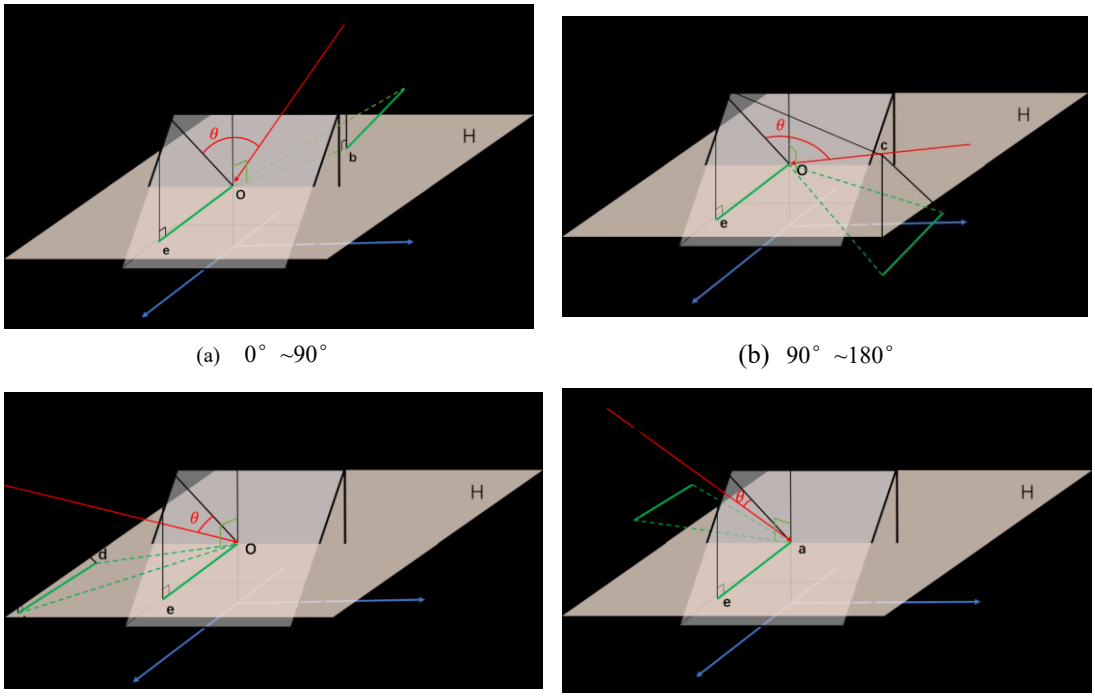

(a) 0° ~90° (b) 90° ~180°

(c) 180° ~270° (d) 270° ~0°

Fig.8 Calculation of cosine of incidence angle in four directions of sunlight reaching a ground surface

(4) Calculation of the solar radiation

Solar irradiance (unit: $\mathrm{w/m^2}$) that can be received at the a given surface location is $Global = Dir + Dif$, where $Dir = \sum Dir_{z,\omega}$ and $Dif = \sum Dif_{z,\omega}$ are direct radiation and diffuse radiation, which are summarized over all sky sectors denoted by zenith angle z and azimuth angle ω. For each sky sector that is not completely obstructed, the direct radiation $Dir_{z,\omega}$ is calculated as follows:

$$Dir_{z,\omega} = S_{Const} \times \beta^{m(z)} \times SunDur_{z,\omega} \times SunGap_{z,\omega} \times cos\theta \quad (6)$$

$$m(z) = exp(-0.000118 \times Elev - 1.638 \times 10^{-9} \times Elev^2)/cos(z) \quad (7)$$

where S_{Const} is the solar constant (1367 $\mathrm{w/m^2}$), β is transmittivity of the atmosphere (averaged over all wavelengths) for the shortest path (in the direction of the zenith), ranging from 0 (no transmission) to 1 (complete transmission). $\beta = 0.5$ indicates a normal clear sky. $m(z)$ is the relative optical path length, measured in proportion to the zenith path length, which is determined by the altitude $Elev$ (unit: m) and zenith angle z. $SunDur_{z,\omega}$ specifies the duration of a sky sector, and the duration represented by each sector is 0.5h. $SunGap_{z,\omega}$ is the ratio of the unobstructed area of that sector. Incidence angle θ is the angle between a surface and incoming radiation reaching the surface. The calculation formula of diffuse radiation corresponding to each sector is as follows:

$$Dif_{z,\omega} = R_{glb} \times P_{dif} \times Dur \times SkyGap_{z,\omega} \times Weight_{z,\omega} \times cos\theta \quad (8)$$

$$R_{glb} = (S_{Const} \sum (\beta^{m(z)}))/(1 - P_{dif}) \quad (9)$$

where R_{glb} represents the global normal radiation ($\mathrm{w/m^2}$), P_{dif} is the proportion of global normal radiation flux that is diffuse, and the value range is [0,1]. Under the condition of very clear sky, the value is about 0.2, and under the condition of extremely thick clouds, the value is about 0.7; Dur is the time interval of analysis; $SkyGap_{z,\omega}$ represents the ratio of the unobstructed area of the sky sector to the sector area; $Weight_{z,\omega}$ represents the proportion of diffuse radiation originating in a given sky sector relative to all sectors, which can be approximately expressed by area ratio. Electric energy converted from solar radiation is calculated as

$$Pow = Global \times Area \times Pho_e \quad (10)$$

where Pow is the power generation (unit: Wh), $Area$ is the area of (unit: $\mathrm{m^2}$), and Pho_e is photoelectric conversion efficiency.

3 Study area and data

3.1 Study area

Qingdao, situated on the coastline of Shandong Peninsula (120°1'E to 120°6'E longitude, 36°N to 36°3'N latitude), is an important coastal center city of China. According to Qingdao Statistical Yearbook[44], by 2019, the city has an urban built-up area of 758.2 $\mathrm{km^2}$, with permanent residents of 9.50 million and the population density of two core municipal administrative regions, i.e., Shinan district and Shibei district, has experienced significant increase, reaching 19,600 person/$\mathrm{km^2}$ and 17,600 person/$\mathrm{km^2}$, respectively. The high-density population living in core areas implies an increase in high-rise buildings, which may result in deep street canyons in narrow areas. On the other hand, the city is characterized by obvious spatial heterogeneity of architectural landscapes due to the diverse development planning and the change of regional function, resulting that eastern region has the lowest land use intensity and the highest average building height; while the western region has the smallest area of open space among buildings and lowest average building height[45]. Qingdao is a representative city with many different styles of street canyons (narrow compacted streets in the urbanized area and wide open streets in the newly-built suburban area). Therefore, this city is suitable as a case study of the potential of solar power generation along bus routes in various streetscapes.

Qingdao has an efficient public transportation network. In 2019, the total length of buses and trolley buses reached 3973 km, transporting more than 1 billion passengers annually[44]. In Qingdao, nearly 99% of origin-destination flows can be transported by public buses in no more than 2 transfers[46]. To meet the demand of sustainable and low-carbon public transportation development, Qingdao government made great efforts to replace conventional diesel buses with clean energy buses in past years. Since the first trial operation of pure electric buses in 2008, the number of pure electric buses in the city reached 2,228 by the end of 2017, accounting for 23% of the city's total number of buses[47], and the average daily operating mileage was close to 150 kilometers[48]. In order to reduce the charging burden on electrical supply, a solar-power charging

pilot project for electric buses was implemented in 2019, i.e., solar panels are installed on the rainproof shed above the charging piles of the bus parking lot, which can meet the electricity demand of 3 to 5 pure electric buses and save cost about RMB¥106,000 per year[49]. In this study, we aim to provide an assessment of solar power generation on the roof of buses fleet covering large-scale urban area, so as to support the decisions on plan and deployment.

3.2 Data collection and processing

The study areas (Shinan, Shibei, Licang, Laoshan and Chengyang) own around 302 bus lines, including regular lines and circle lines. Each direction of travel of a regular line (excluding circle lines) is considered as a separate route due to the different sky views in the two directions. This brings the total number of bus routes to 547. Geographic locations of these bus routes are collected by BIGEMAP software[1]. In order to obtain street-view panorama images along each bus route, we set a specific length of spatial resolution and sample points at that length. The length is set as 50 meters, and a total of 206,433 points are obtained. Due to overlapping of some bus routes, the repeated points are merged, and 31,263 points are obtained after merging. We use them to acquire the panoramic images. Since some sampling points in Baidu Map do not have corresponding panoramas, such as highways, tourist attractions, etc., these sampling points are removed, and finally 28,661 sampling points are retained. Fig.9 (a) shows the distribution of sampling points of the study area. The coordinates of equal interval points on each bus route are used as input for Baidu Map API[2] engines to acquire street-view panoramic images representing a spatial range of 50m surroundings. According to Section 2.2, panoramic images obtained are first transformed to 800×800 fisheye image. We manually labeled 56 fisheye images, and train them on a workstation with NVIDIA GeForce RTX 3080 (10G RAM). Adam optimizer is used with an learning rate as 0.01. The mini-batch size is set to 2 and the epoch is set as 20. Fig.9 (b) illustrates the segmentation results of fisheye images captured at the locations marked in Fig.9 (a).

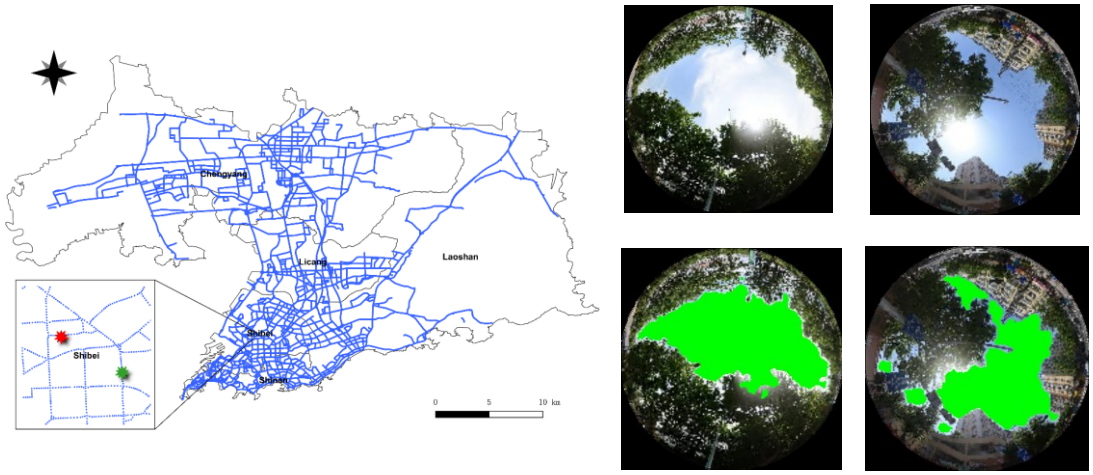

(a) (b)

Fig.9 (a) Spatial distribution of 28,661 street-view panoramic images obtained in the study area; (b) Segmentation results of fisheye images captured at red star and green star in (a)

In order to obtain slope and aspect of a ground surface, DEM data is collected through

[1] www.bigemap.com
[2] https://lbsyun.baidu.com/index.php?title=viewstatic

BIGEMAP software, which is represented as a raster with each grid cell having a surface elevation associated with it. Fig.10 shows the elevation distribution of the study area. Based on elevation data, the slope and aspect of a surface can be calculated by ArcGIS tool. Aspect obtained through ArcGIS starts from due north. In order to calculate the cosine of the incidence angle using Eq. (5), the aspect needs to be rotated to due south. The fisheye image associated with this surface must also undergo the same rotation. The rotation of the fisheye image refers to the azimuth rotation of the center of each sky sector in the Sunmap and the Skymap, but zenith angle remains unchanged. The rotation process is to rotate clockwise when the angle between the aspect and the due south is between 0 and 180 degrees; when the included angle is greater than 180 degrees, counterclockwise rotation.

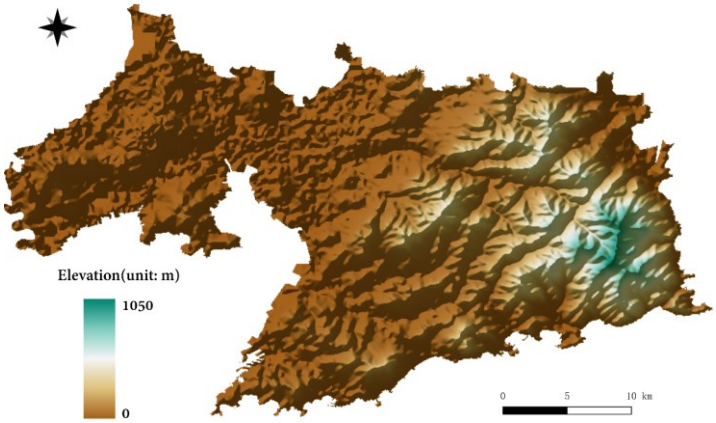

Fig.10 Elevation distribution of the study area

Most of the panoramic images obtained were taken in March. Since the sky view is affected by season (obscured by trees around bus routes), we only study the solar radiation on the day of the spring equinox (March 21). On the spring equinox day, the sunshine time in the study area is about 12 hours during 6:00-18:00. Assuming that the weather on that day is divided into two types, categorized by the percentage of the sky covered by clouds: sunny and cloudy. The clearer weather in Qingdao begins around August 31 and lasts for 5.5 months, ending around February 12. The cloudier part of the year begins around February 12 and lasts for 6.6 months, ending around August 31. The percentages of time spent in each weather type during the year are given in Table 1. The average percentage of cloudy cover is nearly 35% in clearer weather, and that value in cloudier weather is 47%.

Table 1 The percentages of time spent in each weather type, categorized by the percentage of cloud cover

Fraction%	Jan	Feb	Mar	Apr	May	Jun	Jul	Aug	Sep	Oct	Nov	Dec
Cloudier	34	41	46	45	45	46	51	44	37	32	32	30
Clearer	66	59	54	55	55	54	49	56	63	68	68	70

the corresponding P_{dif} are set as 0.4 and 0.6, and β value as 0.5 and 0.3, respectively Detailed information is given in Appendix A.

4. Results

4.1 Spatio-temporal distribution of solar irradiance

For each street-view panoramic image at sampling point (covering 50m space area), the amount of solar irradiance is calculated and accumulated on a sunny day and a cloudy day, respectively. As shown in Fig.11, the highest amount of solar irradiance can reach 7881.96 Wh/m^2 on a sunny day, and the average receiving amount is 5220.02±1638.27 Wh/m^2. A significant decrease of solar radiation is observed in cloudy weather. The maximum solar irradiance is 5948.88 Wh/m^2, and the average value is 3912.58±1157.97 Wh/m^2. This decrease is mainly due to insufficient sunlight caused by the occlusion of clouds in the sky. The direct solar radiation account for about 63.32% of the total solar radiation in sunny day. The proportion drops to 45.68% in a cloudy day, indicating that the generation of solar radiation at a cloudy day mainly relies on diffuse radiation.

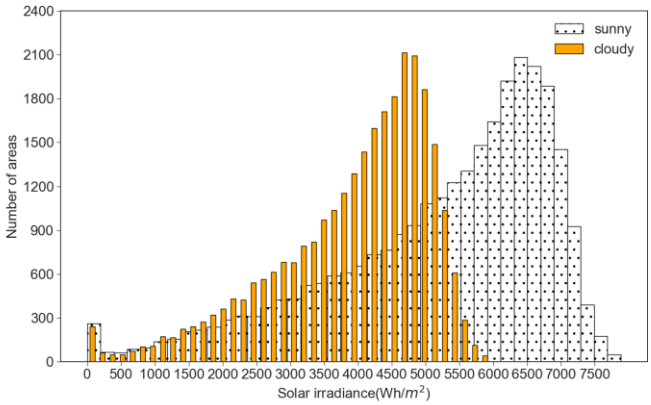

Fig.11 Histogram of solar irradiance generation at a sunny day and at a cloudy day

Fig.12 presents the spatio-temporal distribution of solar radiation in a sunny day (The results of a cloudy day are given in Appendix A). Whether it is sunny or cloudy, the variation of solar irradiance over time first increase from morning to mid-day, and then begins to decrease until sunset. The average solar irradiance at a sunny day increases from 54.55 Wh/m^2 in 6:00-7:00 to 707.29 Wh/m^2 in 11:00-12:00 and then decrease to 41.34 Wh/m^2 in 17:00-18:00; at a cloudy day the value increases from 37.09 Wh/m^2 in cloudy day in 6:00-7:00 to 422.97 and then decreases to 26.99 in 17:00-18:00. The result is consistent with previous studies[50, 51], low solar radiation in the hours near to morning and evening and high at noon.

The spatial distribution of solar radiation shows significant different around the city. Most of the areas receiving high solar radiation are located in northern center of the city, while the southern area of the city associates less solar radiation. The south area is the center of the city, with high-density population and land use density, and is characterized by a denser grid of narrow streets, while the newly built blocks in northern area typically involve a wide and sparse urban network. The deep street canyons in the southern area negatively impact solar radiation reception of that area. The effect of the width of street canyons on the solar radiation was studied in [35]. The authors emphasized the positive relation between the width of roads and the solar radiation. Overall, urban centers receive less solar radiation than rural area, such as a case study in Boston[36] and comparison study of two cities in Brazil[52].


6:00-7:00
Solar irradiance (Wh/m²)
900
600
300
0
0
5
10 km

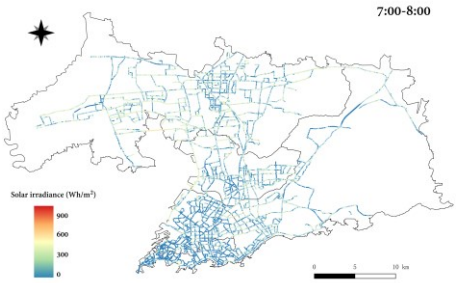
7:00-8:00
Solar irradiance (Wh/m²)
900
600
300
0
0
5
10 km

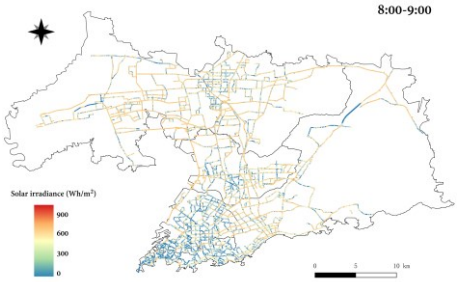
8:00-9:00
Solar irradiance (Wh/m²)
900
600
300
0
0
5
10 km


9:00-10:00
Solar irradiance (Wh/m²)
900
600
300
0
0
5
10 km


10:00-11:00
Solar irradiance (Wh/m²)
900
600
300
0
0
5
10 km

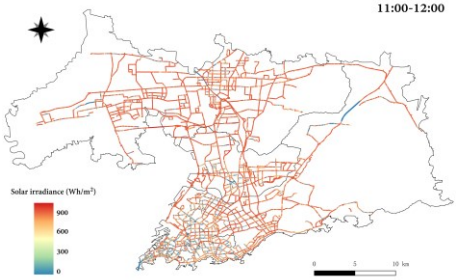
11:00-12:00
Solar irradiance (Wh/m²)
900
600
300
0
0
5
10 km


12:00-13:00
Solar irradiance (Wh/m²)
900
600
300
0
0
5
10 km


13:00-14:00
Solar irradiance (Wh/m²)
900
600
300
0
0
5
10 km

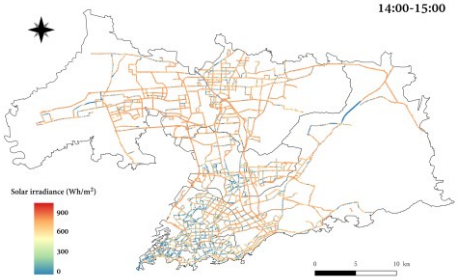
14:00-15:00
Solar irradiance (Wh/m²)
900
600
300
0
0
5
10 km

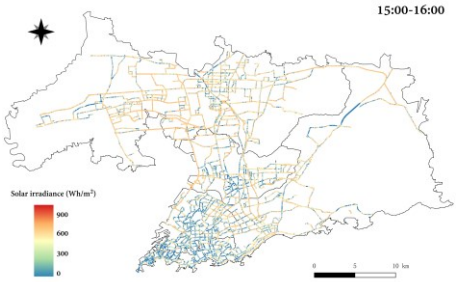
15:00-16:00
Solar irradiance (Wh/m²)
900
600
300
0
0
5
10 km

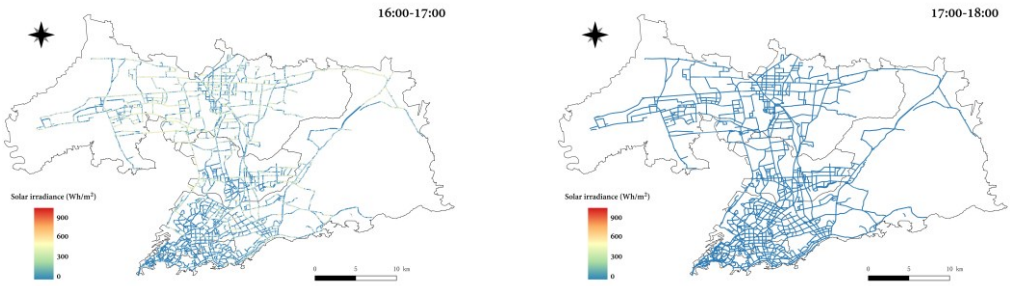

Fig.12 The spatio-temporal distribution of solar radiation in the study area on a sunny day

4.2 Power generation from the received solar radiation of buses

The solar panels are assumed to be installed on rooftop of a bus. The rooftop area is 30m^2 with 12m long and 2.5m wide, a typical bus size in the study area. Similar with [36], the photoelectric conversion efficiency is set as 17% in Eq.(10).

4.2.1 Power generation during operation

For each bus route, we calculate the power generation of a bus during operation at a day. According to our previous study [53-56], the average speed of buses in the study area during peak hours is around 11km/h. Then the travel time of 50m road length (sampling interval) is about 0.3min. This value is used as time interval input in Eq.(6) and Eq.(8). The longer the route, the longer the bus is exposed to solar radiation. In order to avoid cumulative effect of route length, the power generation from solar radiation of a bus is divided by the route length to get the power per kilometer (km).

As shown in Fig.13, the distribution of power generation from solar radiation of operating buses are presented by using a boxplot representation, in which the y-axis represents the power value, and the x axis indicates the time. An inverted U-shape is observed in Fig.11, suggesting a change of the power value from an increase to a decrease overtime. The median value of power generation of a bus per kilometer travel reaches its peak value (350.96Wh on a sunny day and 203.81Wh on a cloudy day) at noon (11:00-13:00), and the smallest value appear (18.54Wh on a sunny day and 12.89Wh on a cloudy day) in the evening (17:00-18:00). The results show that the amount of power generation by a bus per kilometer traveled is positively correlated with the received solar irradiance.

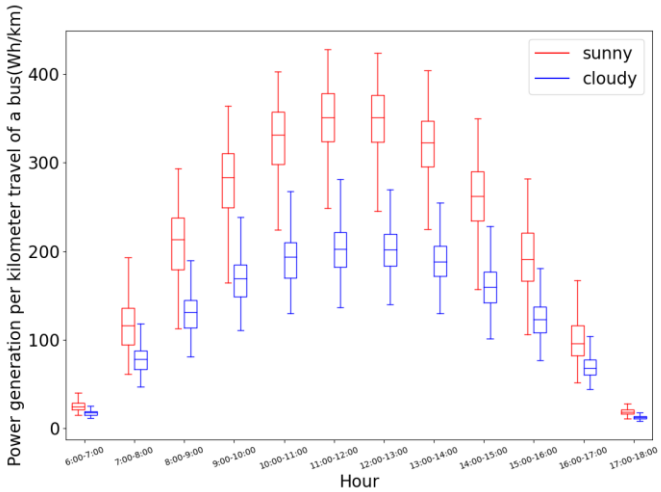

Fig.13 The change of power generation of a bus per meter travel over time on a sunny day and on a cloudy day (outliers bigger than Q3+1.5×IQR* or smaller than Q1-1.5×IQR are omitted)

* IQR: interquartile range, equals to the difference between the 75% median (Q3) and the 25% median (Q1).

According to study [57], for a BYD K9D electric bus (12m-length, in service time < 1 year, and 324 kWh battery capacity), when the air conditioner (AC) is turned off, the electric consumption with half-loaded passengers is 125kWh/100km, and the electric consumption with full-loaded passengers is 136kWh/100km; when the AC is turned on, these values are 145kWh/100km (half-loaded passengers) and 153kWh/100km (full-loaded passengers), respectively. Based on the result of Fig.13, the proportion of power generation from solar radiation to the total electricity consumption demand of a bus traveling one kilometer is calculated in Table 1. In general, the proportion starts to increase in the morning, peaks at noon, and then declines to sunset. Note that, during sunny noon (11:00-12:00), the electricity generated by solar radiation during the operation of a bus accounts for about one-fourth of total electricity consumption of the bus. That percentage drops in a cloudy day, however, it still contributes to one-sixth of total electricity consumption. The electricity from solar radiation can serve as an important supplement to the electricity consumption of buses, and the saving power thereby can be used to increase the driving mileage.

Table 1 The proportion of solar power generation of a bus in operation to the total electricity demand

Time Intervals	Sunny day				Cloudy day			
	HF* with AC* off	FL* with AC off	HF with AC on	FL with AC on	HF with AC off	FL with AC off	HF with AC on	FL with AC on
6:00-7:00	2.06%	1.89%	1.76%	1.68%	1.42%	1.31%	1.22%	1.16%
7:00-8:00	9.44%	8.68%	8.14%	7.71%	6.28%	5.77%	5.41%	5.13%
8:00-9:00	16.78%	15.42%	14.46%	13.71%	10.45%	9.60%	9.01%	8.54%
9:00-10:00	22.38%	20.57%	19.29%	18.28%	13.51%	12.42%	11.64%	11.04%
10:00-11:00	26.25%	24.13%	22.63%	21.44%	15.42%	14.17%	13.29%	12.59%
11:00-12:00	28.03%	25.76%	24.16%	22.90%	16.30%	14.98%	14.05%	13.32%
12:00-13:00	27.96%	25.70%	24.10%	22.84%	16.26%	14.95%	14.02%	13.28%
13:00-14:00	25.67%	23.60%	22.13%	20.97%	15.20%	13.97%	13.10%	12.42%
14:00-15:00	21.06%	19.35%	18.15%	17.20%	12.90%	11.86%	11.12%	10.54%
15:00-16:00	15.67%	14.35%	13.46%	12.75%	9.96%	9.15%	8.58%	8.13%
16:00-17:00	8.13%	7.47%	7.01%	6.64%	5.62%	5.16%	4.84%	4.59%
17:00-18:00	1.53%	1.40%	1.32%	1.25%	1.03%	0.94%	0.88%	0.84%

*HF: half-loaded passengers. FL: full-loaded passengers. AC: air conditioner.

4.2.2 Power generation during stop at parking lot

When electric buses are not in operation, they often stop at a parking lot for charging. Ideally, parking locations should be located in an open space with visible views of the sky from all directions, that is, the gap fraction is 1, where the sunlight reaches the rooftop of a bus without any obscuration. However, limited by urban space, large unobscured parking area is not always feasible. To better understand the power generation capacity on different ratio of visible view of sky at parking locations, 10 equal intervals simulations from 0% to100% are conducted at a sunny day and a cloudy day.

Assuming that the parking lot is located at the end of route, the accumulated power of a bus parked for one hour is calculated, and the average value of total routes is represented by a point in Fig.14, where the color represents the ratio of visible sky area. The power value (1530Wh/km) required for a full-loaded a bus with AC on is marked by a red dotted line. The points above the red dotted line means the accumulated power of one-hour parking can make the full-loaded electric bus with AC on runs for one kilometer. When the ratio of visible sky view at a sunny day is 40%, the one-hour parking duration to meet the electric consumption of the 1km operation spans from 9:00 to 15:00; while the ratio of visible sky view is greater than 70%, the one-hour parking duration can be extended to morning 7:00 and evening 17:00. At a cloudy day, when the ratio of visible sky view is 40%, the one-hour parking duration must be postponed to start at 11:00 and ends early at 13:00 to meet the electricity demand for one kilometer operation with full-loaded passengers and AC turned on. When the ratio of visible sky view is greater than 70%, the one-hour parking duration can be extended between 8:00 and 16:00.

Assuming that a bus stops to acquire solar power from 6:00 to 18:00 and runs at night using the electricity generated by solar radiation during the day. The ratio of visible sky view is set 100%. The accumulated power of a bus can reach 40473Wh at a sunny day, which can extend 25km mileages of a full-loaded passengers bus with AC on to run at night. On cloudy day, as the accumulated power generation of a day decreases to 31299Wh the extended range drops to 20km. During night, the passenger load is rather low, thus the driving range can be further extended to 32km and 25km with half-loaded passengers and AC off.

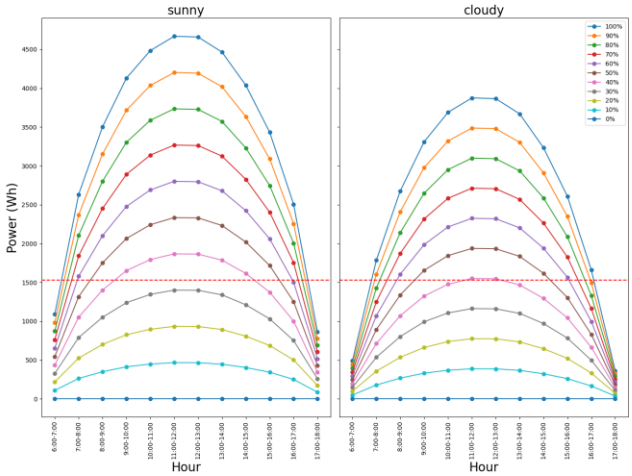

Fig.14 Power generation of a bus at parking lot on a sunny day and cloudy day

4.3 Scenario analysis

4.3.1 Benefits of PV on energy consumption

Limited by battery capacity, it is difficult to achieve a one-by-one replacement for traditional buses with electric buses without increasing operational cost[58]. Practices in Shenzhen, Beijing, Wuhan, Qingdao, and Chongqing showed that 1.5-2 battery-electric buses were needed to provide the same level of services as an existing diesel or CNG bus, and this replacement ratio will be higher when air conditioning is used[59]. In this section, two widely used replacement ratios 2:1 and 4:3 are first discussed. As shown in Fig.15(a), bus A and bus B are electric buses. When one bus is in service, the other one parked at lot, and they provide services alternately, ensuring that one bus

provides service at any time. In Fig.15(b), there are three electric buses (bus A, bus B, bus C) providing service at any time, however, continuous service throughout the day is not possible, and an additional electric bus (bus D) is dispatched to supplement the service. It is obvious that the operation duration of a bus in 2:1 replacement mode is 8 hours and the value of a bus in 4:3 replacement mode is 11-12 hours. When the battery capacity is low, higher replacement ratio (2:1) usually is adopted; while a lower replacement ratio (4:3) usually occurs when the battery capacity is high. However, high replacement ratio means high purchase and maintenance cost.

Noting that the actual start and end time of operation or stops may be different from Fig.15. Considering the convenience of scheduling, the time for each state (operation or stopping) is set as continuous as possible. The following discussion 4.3.2 will show that the start-end time has no influence on the total power generation.

Without loss of generality, we assume: (1) service operation time starts at 6:00 and ends at 21:00; (2) parking lot locates at an open space with visible views of the sky from all directions; (3) power generation from sun radiation during operation and parking duration can be stored and used for extending drive mileage or auxiliary power needs (air conditioner, lighting, passenger information system, etc.); (4) opportunity charging during day are not considered. For each bus route, the power generation of a bus during operation and the power generation in parking lot are calculated, respectively, and for obtaining higher statistical meaning the average value of total routes are used to represent the power generation of buses in Fig.15.

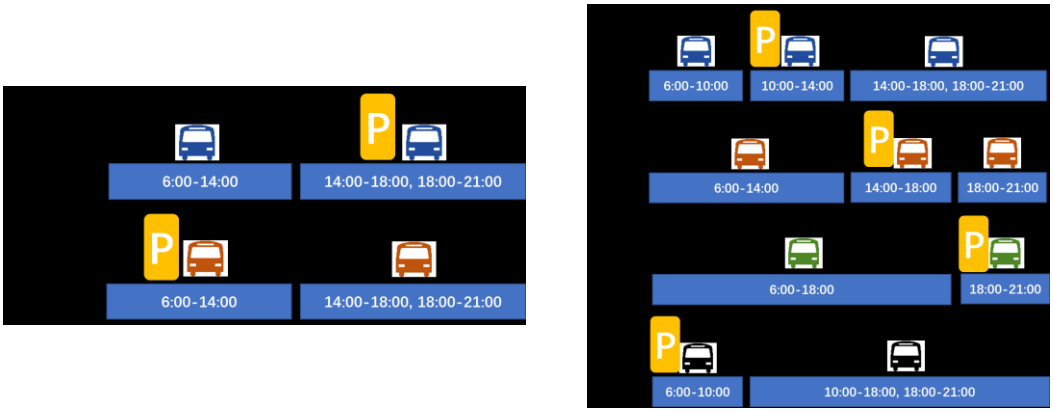

(a) 2:1 replacement (b) 4:3 replacement

Fig.15 Two widely used replacement modes ('P' means parking at lot)

In order to assess the impact of PV on the electrical energy consumption of the bus, we use a BYD K9D electricity bus mentioned in Section 4.2 as an example. The average daily operating mileage of electric buses in Qingdao was close to 150 kilometers [48]. Then the accumulated energy demand of the bus to cover all its journeys in four different modes (HF with AC off, F with AC off, HF with AC on, and FL with AC on) in one day are respectively 229.5kWh, 217.5 kWh, 204 kWh, and 187.5 kWh. The following results of the two replacement modes shown in Fig.15 would reveal how integrated PV power can save energy demand and extend vehicle range. It is worth noting that installing solar panels on the roof will increase the body weight and cause more power consumption. Monocrystalline and polycrystalline solar panels are the two most common types of solar energy receptors, and both are lightweight and flexible photovoltaic modules. Based on manufacturer data[14], the area density of a crystalline silicon PV module is 1.89 kg/m^2, then the extra mass

caused by solar panels installed on the roof (30 m^2) of a bus is 56.7 kg, which is similar with a weight of an adult passenger. More recently, flexible thin film solar cells, with the advantage of being much thinner (10μm or less instead of about 300μm of crystalline silicon) and requiring less material, are considered to have more important applications on vehicles[60]. Therefore, the entire PV modules have little effect on the total vehicle mass, thus contributing minimal additional weight or wind resistance.

For bus A in 2:1 replacement mode, the power generating from solar radiation when operation in a sunny day (6:00-14:00) is 21808.33Wh, and the value is 10838.88Wh when it stops at lot (14:00-18:00); for bus B, the power generation when it stops at lot in a sunny day (6:00-14:00) is 29634.53Wh, and the value when it is during operation (14:00-18:00) is 6372.35Wh. The total power generation of these two buses are 68654.09Wh, and the average value per bus is 34327.04Wh. The energy demand per bus reduces to 195.17kWh, 183.18kWh, 169.67kWh and 153.17kWh, respectively, and the saving energy demand can be used to extend 22.43km, 23.67km, 25.24km and 27.46km driving range. The average length of routes in the study area is 18.73km, that is, the power can make a bus travel one more circuit at least.

In 4:3 replacement mode, the power generating from solar radiation of bus A is 6967.41Wh (6:00-10:00), 18279.55Wh (10:00-14:00), and 6372.35Wh (14:00-18:00); the power generation of bus B is 21808.33Wh (6:00-14:00) and 10838.88Wh (14:00-18:00); the power generation of bus C is 28180.69Wh (6:00-18:00); the power generation of bus D is 11354.98Wh (6:00-10:00) and 21213.28Wh (10:00-18:00). The total power of these four buses is 125018.47Wh, and the average value per bus is 31254.61Wh, which is a little lower than the value of 2:1 replacement mode. For a PV-integrated electricity bus in 4:3 replacement mode, the energy demand per bus reduces to 198.24 kWh, 186.24 kWh, 172.74 kWh and 156.24 kWh, respectively, and The driving range of a bus in 4:3 replacement mode can be extended correspondingly 20.42km, 21.55km, 22.98km, and 25km under the four different operation modes as mentioned above (half/full loaded passengers and AC off/on).

4.3.2 Impact of replacement ratio on energy consumption

Let *m* and *n* be the number of conventional buses and electric buses, respectively. $r = n/m$ is the replacement ratio of electric buses to conventional buses. Obviously, $r \geq 1$. $r = 1$ means one-by-one replacement. The average power generation from solar radiation of an electric bus can be calculated as

$$\frac{\sum_{i=1}^{12} mp_i + (n-m)q_i}{n} \tag{11}$$

where *i* is a time interval and a day (6:00-18:00) is divided into 12 intervals. p_i and q_i are the power generation from solar radiation when the bus is in operation and when it stops at a lot, respectively, in the time interval *i*. When r=2 (2:1 replacement mode), the average power generation from solar radiation of a bus is $\sum_{i=1}^{12} 2p_i + q_i$; when r=4/3 (4:3 replacement mode), the average power generation from solar radiation of a bus is $\sum_{i=1}^{12} 4p_i + q_i$. With $n = mr$, Eq.(11) can be rewritten as

$$\frac{1}{r}\sum_{i=1}^{12} p_i + (1-\frac{1}{r})\sum_{i=1}^{12} q_i \tag{12}$$

With given replacement ratio $r \in [1,2]$, the average power generation from solar radiation of a bus is shown in Fig.16. The average power generation from solar radiation of a bus increase with

the r value, and reaches the maximum value (34327.06Wh in a sunny day and 24167.09 in a cloudy day) when $r = 2$. The result suggests that the high cost of 2:1 replacement can be greatly reduced by the power supplement of solar radiation.

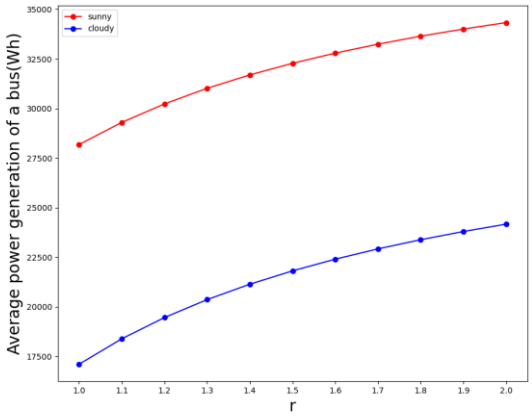

Fig.16 The change of average power generation of a bus with replacement ratio r

5. Discussion and implications

This paper discusses an alternative solution for integrating PV modules on the body of an electric bus as an auxiliary power source, which can keep battery charged and reduce the load of power grid. We assume that solar PV panels are installed on rooftops of an electric bus that is 12m long and 2.5m wide. For each route, power generation from solar radiation received by the PV panels on a bus in operation service is estimated.

Results show that amount of power is positively correlated with the received solar irradiance, i.e. it increases from the morning, peaks at noon, and then decreases until sunset (Fig.13). Note that a large electricity demand of battery units occurs during in morning and evening peak hours, which is caused by a large number of passengers on board and the low speed driving[61]. The surging electricity consumption for driving during the morning peak hours can be supplemented in real time by solar radiation, and the supplementary amount reaches its peak at noon. Results in Table 1 show that the electricity generated by solar radiation accounts for about 28.03%, 22.90% of total electricity consumption of a bus at sunny noon, when it transports half-loaded passengers with AC turned off, and full-loaded passengers and AC turn on, respectively. This can significantly reduce the risk of deep discharge of battery during operation in rush hours and improve the cycle life of the battery. Considering the real-time charging advantages of solar radiation, roof-mounted PV as auxiliary power source can be an effective approach to make up for the high cost and limited route flexibility of opportunity charging end-of-route or en-route.

In [22], the authors argued that buses that can use highway with fewer shadowing and a steady velocity have more PV power generation than these only traveling in downtown areas. Spatial distribution of power generation in our case study confirm this conclusion. Huanwan Road is an expressway close to Jiaozhou Bay, connecting the north and south of the city. Route 761 and 765 travel along this expressway, and the peak values of power generation of a bus per kilometer travel are 413.58Wh/km and 401.53Wh/km, respectively, which are nearly 1.2 times of the average peak value (349.56Wh) of total routes in the city. Here, another interesting finding is that routes driven in newly-launched areas also have power generation advantages. For example, route 914 and 207

driven in the newly built blocks in northern area, and our results show that the peak values of power generation of these four routes are 758.09Wh/km and 756.59Wh/km, which are much higher than routes driven along expressway, and 2.16 times the average level. The results suggest that urban areas with wide and sparse urban network are more suitable to employ PV-integrated buses. Located in northern temperate monsoon zone, Qingdao has weak advantage of solar irradiation compared with areas close to the equator. As a result, when considering the potential of PV-integrated electric buses, newly-built urban areas with sparse road network should give priority to pilot project. However, for areas with abundant solar radiation, this requirement can be relaxed. For example, a trial project of solar-powered buses with ultra-thin PV panels mounted on the roofs has been launched in Singapore. Therefore, we suggest a comprehensive consideration of latitude and urban architectural landscapes when planning the deployment of PV-integrated electric buses in different cities, i.e. solar-powered buses are still attractive in the downtown of low-latitude cities.

By now, electric buses cannot drive the same mileage compared with conventional diesel or CNG buses due to limited battery capacity. Replacement ratios of 2:1 and 4:3 are widely employed in many cities (Fig.15). We discuss the average amount of generating solar power that can be used for operation through alternatively service (on-duty on road and off-duty at parking lot). The saving charging from power grid is evaluated by summing solar power generation while driving and parking. Considering the average route length in the study area is 18.73km, with 2:1 replacement schedule, the solar power generated in a sunny day can make a bus full of passengers and with AC on at least one extra trip (22.43km); while with 4:3 replacement schedule, the length of extended mileage is 20.42km. We define replacement ratio as the proportion of the number of electric buses to the number of conventional buses. The relation between the replacement ratio and the average solar power generation of a bus is given in Eq. (12). One interesting finding is the power supplementary increases with the replacement ratio (Fig.16), and peaks at 2:1 replacement ratio. The main reason is that more stopping time occurs in this mode, and the solar power produced is higher when stopping at parking lot than when driving around the city. The results are based on the assumption of open parking lot with no sky obscuration. Although the open parking lot is not always feasible in downtown area, the results provide meaningful insights. Due to significant energy consumption difference between energy usage with and without AC[62], it is difficult for long-distance routes to achieve a low replacement ratio in summer or winter, so the 2:1 replacement mode is still dominated in near future, resulting in high purchase and maintenance cost. Therefore, our finding suggests a promising approach to reduce the high cost of 2:1 replacement by replenishing electricity in real time through solar radiation. Although an economic analysis was not conducted in the present investigation, the energy generation during electric bus operations and parking can be expected to offset some costs associated with the power purchase from grid.

The experimental results reveal how integrated PV power can improve operational performance of electric buses, such as extending driving range or saving energy demand. However, some argue that there are other alternatives, such as simply using a larger battery or optimizing service schedules. Previous studies showed that the benefits of integrated PV held up against the benefits of other alternatives. For example, simulation study of an electric bus on a suburban bus route in Davis, CA, USA validated that on-board PV modules can extend battery cycle life by up to 10%-19% compared with expanding the size of battery [14]; PV-integrated buses can make a significant reduction in load during peak times of the day, that is, lower loads on distribution transformers and thus lower aging[63]. Although the result was concluded by one week driving data

of 150 car drivers, this revealed the grid benefits by introducing PV-integrated bus fleet. In addition, as a supplementary power source, integrated PV can provide electric power for passenger information systems, ticket vending machines and USB chargers so as to reduce the energy consumption of battery. This way, integrated PV has better prospects in promoting sustainable public transport.

Up to now, cost is one of the main reasons for not using PV-integrated vehicles on a large scale. However, the installed cost of PV modules and battery storage systems continued to drop in recent years. The average price for CIGS PV modules, a main thin film solar technology, fell from $4/W in 2007 to $0.4/W in 2017 [64]. Now, the extra cost of PV modules installed on bus roofs becomes affordable. Research work in 2012 showed that the payback period required for the installation cost of various PV modules (crystalline silicon, polycrystalline silicon and thin film) were 4.1 years, 4.6 years and 4.6 years, respectively[60]. Due to the decline in price the payback period is expected to be shortened now and even further in the future.

6. Conclusion

Accurate estimation of the potential of solar PV of electric buses is important prerequisite for better planning of sustainable public transport. This study focuses on developing a method framework with detailed procedure for estimating solar radiation-generated electricity energy of fleet-wide PV-integrated electric buses traveling around city-wide area. The framework gives detailed procedure on street-view panoramas acquisition, hemispherical projection from panoramas to fisheyes images, fisheye images segmentation, solar radiation calculation (estimation of gap fraction and incidence angle). Taking Qingdao, China as example, a possibility of integration PV modules on electric buses as an auxiliary power source for real-time charging is studied in this paper. Spatio-temporal pattern of solar radiation is quantified, and the potential power generation of PV-integrated electric buses on-duty in the roads and off-duty in the parking lot is analyzed. The power generation benefit of different replacement schedules is discussed in scenario analysis. The key points from this study are:

- The electricity consumption during operation can be supplemented in real time by solar radiation, and the supplementary amount reaches its peak at noon, which can reduce the risk of deep discharge.
- The spatial variability of power generation from solar radiation suggests that routes driven in newly-launched areas and expressway have significant power generation advantages.
- It is observed that the power generation benefit is highly correlated with the replacement ratio. The solar power generated in a sunny day can make a bus full of passengers and with AC on at least one extra trip in 2:1 replacement mode and 4:3 replacement mode.
- The high cost of 2:1 replacement can be reduced by replenishing electricity in real time through solar radiation, which providing a feasible solution for long-distance routes during summer or winter.

Our study provides an effective approaching for the potential analysis of PV-integrated electric buses. The method framework proposed in this paper can be easily applied to cities with available coverage of street view panoramas, and DEM data. The results of case study can be used to understand the feasibility of fleet-wide planning of PV-integrated buses to support effective decisions at city-wide scale. In future, real electricity consumption of buses under complex transport

conditions[65-67] and travel behaviors change[68] will be collected in order to give a more detailed analysis of the economic benefits of solar power generation.

Acknowledgements

This research is supported by Young Scientists Fund of the National Natural Science Foundation of China (41706198), Beijing Natural Science Foundation Grant L211027, and Qingdao Independent innovation major special project (21-1-2-1hy).

Appendix A

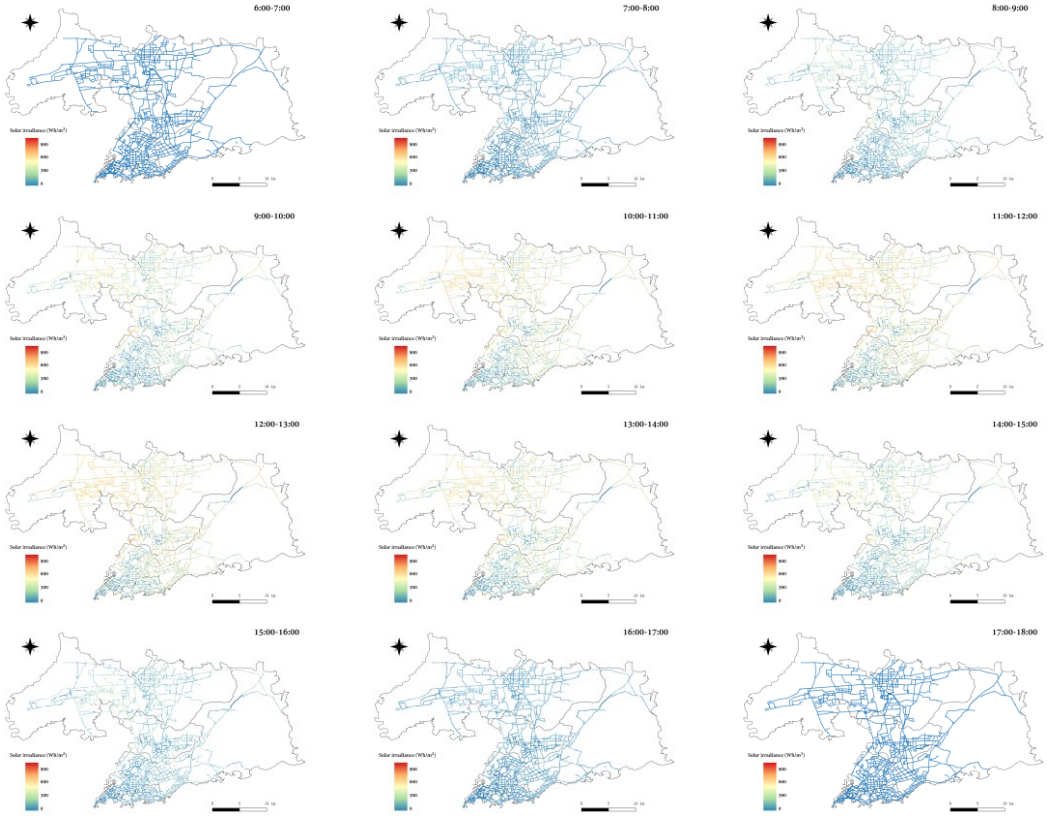

Fig.A1 The spatio-temporal distribution of solar radiation in the study area on a cloudy day

Reference:

[1] Rogelj J, Luderer G, Pietzcker RC, Kriegler E, Schaeffer M, Krey V, et al. Energy system transformations for limiting end-of-century warming to below 1.5 C. Nature Climate Change. 2015;5:519-27.

[2] R. S, Schaeffer R, Creutzig F, Cruz-Núñez X, D'Agosto M, Dimitriu D, et al. Transport. In: Climate Change 2014: Mitigation of Climate Change. Contribution of Working Group III to the Fifth Assessment Report of the Intergovernmental Panel on Climate Change; 2014.

[3] Wang C, Cai W, Lu X, Chen J. CO2 mitigation scenarios in China's road transport sector. Energy Conversion and Management. 2007;48:2110-8.

[4] Weiss M, Dekker P, Moro A, Scholz H, Patel MK. On the electrification of road transportation–a review of the environmental, economic, and social performance of electric two-wheelers. Transportation Research Part D: Transport and Environment. 2015;41:348-66.

[5] IEA CEM. Global EV outlook 2019. IEA: Paris, France. 2019.
[6] Heid B, Kasser M, Muller T, Pautmeier S. Fast transit: Why urban e-buses lead electric-vehicle growth. McKinsey & Company.
[7] Grütter J, Frecon A, Ferreira A, Gong L, Song L, Wang J, et al. SUSTAINABLE TRANSPORT SOLUTIONS: Low-Carbon Buses in the People's Republic of China. Asian Development Bank; 2018.
[8] Transport Ma. European Clean Bus deployment Initiative. European Commission.
[9] Innovative Clean Transit (ICT) Regulation Fact Sheet. California Air Resources Board; 2018.
[10] Borozan S, Giannelos S, Strbac G. Strategic network expansion planning with electric vehicle smart charging concepts as investment options. Advances in Applied Energy. 2022;5:100077.
[11] Vepsäläinen J, Ritari A, Lajunen A, Kivekäs K, Tammi K. Energy uncertainty analysis of electric buses. Energies. 2018;11:3267.
[12] Bartłomiejczyk M, Kołacz R. The reduction of auxiliaries power demand: The challenge for electromobility in public transportation. Journal of Cleaner Production. 2020;252:119776.
[13] Gallet M, Massier T, Hamacher T. Estimation of the energy demand of electric buses based on real-world data for large-scale public transport networks. Applied energy. 2018;230:344-56.
[14] Mallon KR, Assadian F, Fu B. Analysis of on-board photovoltaics for a battery electric bus and their impact on battery lifespan. Energies. 2017;10:943.
[15] Gao Z, Lin Z, LaClair TJ, Liu C, Li J-M, Birky AK, et al. Battery capacity and recharging needs for electric buses in city transit service. Energy. 2017;122:588-600.
[16] Bi Z, De Kleine R, Keoleian GA. Integrated Life Cycle Assessment and Life Cycle Cost Model for Comparing Plug-in versus Wireless Charging for an Electric Bus System. Journal of Industrial Ecology. 2017;21:344-55.
[17] Bi Z, Song L, De Kleine R, Mi CC, Keoleian GA. Plug-in vs. wireless charging: Life cycle energy and greenhouse gas emissions for an electric bus system. Applied Energy. 2015;146:11-9.
[18] Liu L, Kong F, Liu X, Peng Y, Wang Q. A review on electric vehicles interacting with renewable energy in smart grid. Renewable and Sustainable Energy Reviews. 2015;51:648-61.
[19] Assadian F, Mallon KR, Fu B. The Impact of Vehicle-Integrated Photovoltaics on Heavy-Duty Electric Vehicle Battery Cost and Lifespan. SAE Technical Paper; 2016.
[20] Geca M, Wendeker M, Grabowski L. A City Bus Electrification Supported by the Photovoltaic Power Modules. SAE Technical Paper; 2014.
[21] Muttana SB, Dey RK, Sardar A. Prospects of Electric Bus Integrated with Solar Photovoltaic Cells. SAE Technical Paper; 2017.
[22] Oh M, Kim S-M, Park H-D. Estimation of photovoltaic potential of solar bus in an urban area: Case study in Gwanak, Seoul, Korea. Renewable Energy. 2020;160:1335-48.
[23] ur Rehman N, Hijazi M, Uzair M. Solar potential assessment of public bus routes for solar buses. Renewable Energy. 2020;156:193-200.
[24] Masuda T, Araki K, Okumura K, Urabe S, Kudo Y, Kimura K, et al. Static concentrator photovoltaics for automotive applications. Solar Energy. 2017;146:523-31.
[25] Data and software architects for bankable solar investments.
[26] AS TaD.
[27] National Solar Radiation Database.
[28] Freitas S, Catita C, Redweik P, Brito MC. Modelling solar potential in the urban environment: State-of-the-art review. Renewable and Sustainable Energy Reviews. 2015;41:915-31.
[29] Watson I, Johnson G. Graphical estimation of sky view-factors in urban environments. Journal

of climatology. 1987;7:193-7.
[30] Oke TR. Street design and urban canopy layer climate. Energy and buildings. 1988;11:103-13.
[31] Liang J, Gong J, Sun J, Zhou J, Li W, Li Y, et al. Automatic sky view factor estimation from street view photographs—A big data approach. Remote Sensing. 2017;9:411.
[32] Gong F-Y, Zeng Z-C, Zhang F, Li X, Ng E, Norford LK. Mapping sky, tree, and building view factors of street canyons in a high-density urban environment. Building and Environment. 2018;134:155-67.
[33] Gong F-Y, Zeng Z-C, Ng E, Norford LK. Spatiotemporal patterns of street-level solar radiation estimated using Google Street View in a high-density urban environment. Building and Environment. 2019;148:547-66.
[34] Li X, Ratti C, Seiferling I. Quantifying the shade provision of street trees in urban landscape: A case study in Boston, USA, using Google Street View. Landscape and Urban Planning. 2018;169:81-91.
[35] Liu Y, Zhang M, Li Q, Zhang T, Yang L, Liu J. Investigation on the distribution patterns and predictive model of solar radiation in urban street canyons with panorama images. Sustainable Cities and Society. 2021:103275.
[36] Liu Z, Yang A, Gao M, Jiang H, Kang Y, Zhang F, et al. Towards feasibility of photovoltaic road for urban traffic-solar energy estimation using street view image. Journal of Cleaner Production. 2019;228:303-18.
[37] Fu P, Rich PM. Design and implementation of the Solar Analyst: an ArcView extension for modeling solar radiation at landscape scales. Proceedings of the nineteenth annual ESRI user conference: San Diego USA; 1999. p. 1-31.
[38] Ronneberger O, Fischer P, Brox T. U-net: Convolutional networks for biomedical image segmentation. International Conference on Medical image computing and computer-assisted intervention: Springer; 2015. p. 234-41.
[39] Li P, Zhang H, Guo Z, Lyu S, Chen J, Li W, et al. Understanding rooftop PV panel semantic segmentation of satellite and aerial images for better using machine learning. Advances in Applied Energy. 2021;4:100057.
[40] Zhang Z, Qian Z, Zhong T, Chen M, Zhang K, Yang Y, et al. Vectorized rooftop area data for 90 cities in China. Scientific Data. 2022;9:66.
[41] Coors B, Condurache AP, Geiger A. Spherenet: Learning spherical representations for detection and classification in omnidirectional images. Proceedings of the European conference on computer vision (ECCV)2018. p. 518-33.
[42] Sekkat AR, Dupuis Y, Honeine P, Vasseur P. A comparative study of semantic segmentation using omnidirectional images. Congrès Reconnaissance des Formes, Image, Apprentissage et Perception (RFIAP)2020.
[43] Rich P, Dubayah R, Hetrick W, Saving S. Using viewshed models to calculate intercepted solar radiation: applications in ecology. American Society for Photogrammetry and Remote Sensing Technical Papers. American Society of Photogrammetry and Remote Sensing1994. p. 524-9.
[44] Bureau QMS, Qingdao NSOi. 2020 Qingdao Statistical Yearbook. 2019.
[45] Zhang P. Spatiotemporal features of the three-dimensional architectural landscape in Qingdao, China. Plos one. 2015;10:e0137853.
[46] Sui Y, Shao F, Yu X, Sun R, Li S. Public transport network model based on layer operations. Physica A: Statistical Mechanics and its Applications. 2019;523:984-95.

[47] Lulu X, Dazizong L, Wei W, Liu P. Overcoming the operational challenges of electric buses: lessons learnt from China. 2019.
[48] Sciences CAoT. China's Experience in Promoting and Applying New Energy Urban Buses. 2020.
[49] Daily QF. Qingdao's first public transportation photovoltaic power station opens. http://eastmoney.com; 2019.
[50] Koudouris G, Dimitriadis P, Iliopoulou T, Mamassis N, Koutsoyiannis D. Investigation on the stochastic nature of the solar radiation process. Energy Procedia. 2017;125:398-404.
[51] Alonso-Montesinos J, Batlles FJ. Solar radiation forecasting in the short-and medium-term under all sky conditions. Energy. 2015;83:387-93.
[52] Codato G, Oliveira A, Soares J, Escobedo JF, Gomes E, Pai A. Global and diffuse solar irradiances in urban and rural areas in southeast Brazil. Theoretical and Applied Climatology. 2008;93:57-73.
[53] Sui Y, Zhang H, Shang W, Sun R, Wang C, Ji J, et al. Mining urban sustainable performance: Spatio-temporal emission potential changes of urban transit buses in post-COVID-19 future. Applied Energy. 2020;280:115966.
[54] Bi H, Shang W-L, Chen Y, Wang K, Yu Q, Sui Y. GIS aided sustainable urban road management with a unifying queueing and neural network model. Applied Energy. 2021;291:116818.
[55] Shang W-L, Chen Y, Li X, Ochieng WY. Resilience Analysis of Urban Road Networks Based on Adaptive Signal Controls: Day-to-Day Traffic Dynamics with Deep Reinforcement Learning. Complexity. 2020;2020.
[56] Shang W-L, Chen Y, Bi H, Zhang H, Ma C, Ochieng WY. Statistical characteristics and community analysis of urban road networks. Complexity. 2020;2020.
[57] Song Q, Wang Z, Wu Y, Li J, Yu D, Duan H, et al. Could urban electric public bus really reduce the GHG emissions: A case study in Macau? Journal of Cleaner Production. 2018;172:2133-42.
[58] Verbrugge B, Hasan MM, Rasool H, Geury T, El Baghdadi M, Hegazy O. Smart Integration of Electric Buses in Cities: A Technological Review. Sustainability. 2021;13:12189.
[59] Li B. Research on operation evaluation system of new energy public transport vehicles. 2018.
[60] Giannouli M, Yianoulis P. Study on the incorporation of photovoltaic systems as an auxiliary power source for hybrid and electric vehicles. Solar Energy. 2012;86:441-51.
[61] He X, Zhang S, Ke W, Zheng Y, Zhou B, Liang X, et al. Energy consumption and well-to-wheels air pollutant emissions of battery electric buses under complex operating conditions and implications on fleet electrification. Journal of cleaner production. 2018;171:714-22.
[62] Göhlich D, Fay T-A, Jefferies D, Lauth E, Kunith A, Zhang X. Design of urban electric bus systems. Design Science. 2018;4.
[63] Mobarak MH, Kleiman RN, Bauman J. Solar-charged electric vehicles: A comprehensive analysis of grid, driver, and environmental benefits. IEEE Transactions on Transportation Electrification. 2020;7:579-603.
[64] Ramanujam J, Bishop DM, Todorov TK, Gunawan O, Rath J, Nekovei R, et al. Flexible CIGS, CdTe and a-Si: H based thin film solar cells: A review. Progress in Materials Science. 2020;110:100619.
[65] Shang W-L, Gao Z, Daina N, Zhang H, Long Y, Guo Z, et al. Benchmark analysis for robustness of multi-scale urban road networks under global disruptions. IEEE Transactions on Intelligent Transportation Systems. 2022.
[66] Shang W-L, Chen Y, Song C, Ochieng WY. Robustness analysis of urban road networks from

topological and operational perspectives. Mathematical Problems in Engineering. 2020;2020.
[67] Shang W-L, Chen Y, Ochieng WY. Resilience analysis of transport networks by combining variable message signs with agent-based day-to-day dynamic learning. IEEE Access. 2020;8:104458-68.
[68] Zhang H, Chen J, Yan J, Song X, Shibasaki R, Yan J. Urban power load profiles under ageing transition integrated with future EVs charging. Advances in Applied Energy. 2021;1:100007.